ChemComm

COMMUNICATION

View Article Online
View Journal | View Issue

Cite this: *Chem. Commun.*, 2021, **57**, 11964

Received 14th September 2021,
Accepted 18th October 2021

DOI: 10.1039/d1cc05182b

rsc.li/chemcomm

Improved catalytic hydrogen release of quasi HKUST-1 compared to HKUST-1†

Minoo Bagheri,[a] Arianna Melillo,[b] Belen Ferrer,[b] Mohammad Yaser Masoomi*[a] and Hermenegildo Garcia *[b]

On-demand hydrogen release could be an important process for the transportation of fuel in the near future. Herein it is reported that the controlled thermolysis of HKUST-1 under optimal conditions generates structural defects resulting in a quasi-HKUST-1 material showing a 20-fold enhancement of the H_2 release turnover frequency at room temperature in the absence of a base.

Green hydrogen is considered an ideal energy storage and carrier compound. Hydrogen is an abundant element and its molecule is a clean energy vector that forms environmentally friendly by-products and has a high combustion energy of 120 MJ kg^{-1}, which is higher than that of diesel and gasoline (46 MJ kg^{-1}).[1] In the past, several techniques have been applied for hydrogen generation including electrolysis,[2] water splitting,[3,4] and chemocatalytic hydrogen generation reactions (HGR).[1] Chemocatalytic HGR is an efficient method of transportation for on-board hydrogen release.

In this context, the catalytic hydrolysis of hydrides or their decomposition under mild reaction conditions, is one of the most convenient methods for H_2 release. For this purpose, sodium borohydride ($NaBH_4$) is a suitable HGR compound, since it has a high H_2 capacity (10.8 wt%) and provides a high purity of evolved H_2 and high H_2 production rates.[1] Most studies have been carried out on the use of expensive and scarce noble catalysts such as ruthenium and platinum.[5–7] Alternative affordable catalysts exhibiting high efficiency and stability are highly wanted in this area.

Metal–organic frameworks (MOFs), constituted by metal ions/clusters and organic linkers, which have coordinatively unsaturated metal sites, have been found to be highly active heterogeneous catalysts.[8–11] Unfortunately, the catalytically active sites in some MOFs are not accessible due to diffusion limitations.[12,13] Pore engineering and defect generation have become a general strategy to increase diffusion rates and site accessibility in MOFs.[10,14–16] In this context, the controlled thermal deligandation process to create Lewis acid centres at structural defects and additional porosity can be a suitable general procedure to increase the porosity and density of the Lewis acid sites in MOFs. The materials resulting after the controlled thermolysis have been denoted as quasi-MOFs (Q-MOFs),[17–20] since they represent a transition between highly crystalline materials and the corresponding metal oxides.[21]

Herein, the controlled thermal treatment of HKUST-1 (Cu_3BTC_2, BTC: 1,3,5-benzenetricarboxylic acid), which renders a material with enhanced catalytic activity for HGR using $NaBH_4$ hydrolysis, is reported. It will be shown that the controlled thermal treatment of HKUST-1 can create concurrent distribution of both micro and mesopores together with an extra density of open coordinatively unsaturated copper sites in the resulting quasi-HKUST, with both factors contributing to the observed high catalytic activity.

HKUST-1 was synthesized by mixing copper(II) acetate and a BTC ligand in a 1-to-1 mixture of H_2O and EtOH in a round bottom flask at 110 °C for 4 h (see the ESI,† Fig. S1). The framework of HKUST has square-shaped pores (9 Å × 9 Å) with six coordinated Cu(II) metal centers. The coordination environment of each Cu(II) comprises four oxygen atoms from four BTC ligands with an additional Cu–Cu bond (2.628 Å) and one coordinated H_2O molecule along the Cu–Cu axis direction (Fig. 1a). The bonded H_2O can be removed *via* thermal treatment under vacuum, as it is H_2O exchangeable and does not compromise the lattice structure.

Considering the TGA profile (Fig. S3, ESI†), different temperatures of 200, 240, 260, and 300 °C were chosen for the thermal treatment of HKUST-1 to generate structural defects, and created unsaturated inorganic nodes and additional porosity. Analysis of the exhaust gases during the thermal process upon heating at 240 °C for 1 h shows the presence of H_2O and

[a] *Department of Chemistry, Faculty of Science, Arak University, Arak 3848177584, Iran. E-mail: m.y.masoomi@gmail.com*
[b] *Instituto Universitario de Tecnología Química Consejo Superior de Investigaciones Científica-Universitat Politecnica de Valencia and Departamento de Química, Universitat Politecnica de Valencia, Av. de los Naranjos s/n, 46022 Valencia, Spain. E-mail: hgarcia@upv.es*

† Electronic supplementary information (ESI) available. See DOI: 10.1039/d1cc05182b

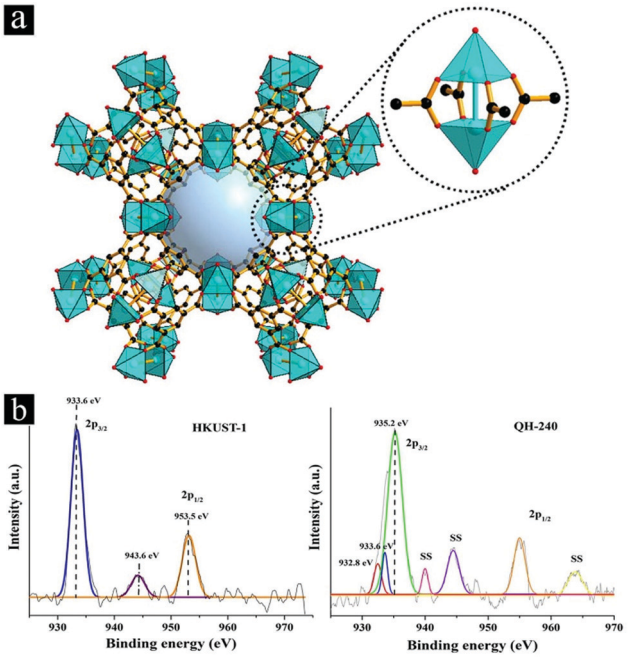

Fig. 1 (a) Single-crystal X-ray structure of HKUST-1. Color code: O, red; C, black; and Cu, blue. (b) Fitted XP spectra of the Cu 2p peaks for HKUST-1 and QH-240 (SS = shake up satellite).

CO_2 in a 5 : 1 ratio, indicating the removal of the H_2O ligands and the partial thermal decarboxylation of the BTC linkers. The dimensions and shape of the QH-*x* particles present in the powders were studied using FE-SEM, which shows a decrease in particle size during the thermal treatment. The HKUST sample is constituted from nanorods (Fig. S4, ESI†). Thermal treatment at 240 °C leads to agglomeration of the small particles to form larger crystallites (Fig. S4, ESI†).

The XPS analysis for HKUST-1 shows that for Cu $2p_{3/2}$ and Cu $2p_{1/2}$ two peaks are located at 933.6 and 953.5 eV and the corresponding Cu $2p_{3/2}$ shakeup satellite is located about 10 eV higher, all of which belong to Cu^{2+} (Fig. 1b).[22,23] For QH-240, two new peaks at 932.8 and 935.2 eV appeared and are attributed to Cu^{+} and Cu^{2+} in a tetrahedral coordination, respectively, with a concomitant significant decrease in the peak intensities of octahedral Cu^{2+} (8%).[24] The XPS results confirm that a minor fraction of Cu^{+} (8%) is generated in QH-240 after deligandation together with tetrahedral Cu^{2+} sites (84%).

The PXRD pattern results confirm the stability of the framework up to 240 °C with a slight broadening and decrease in the intensity of the diffractions in the rage of 5°–10°, which indicates the preliminary deligandation of HKUST. The increase in peak width can be associated with the decrease in particle size as observed using SEM. Upon increasing the temperature to 260 °C the intensity of the characteristic peaks considerably decrease and disappear, which demonstrates destruction of the framework and the formation of Cu_2O/CuO (JCPDS No. 05-0667 and 48-1548). Finally, HKUST-1 is completely converted to CuO at 300 °C (Fig. 2).

For the catalytically most active sample QH-240 (*vide infra*), thermal treatment and partial deligandation causes the formation of fine CuO*x* nanoparticles of about a 10 nm average

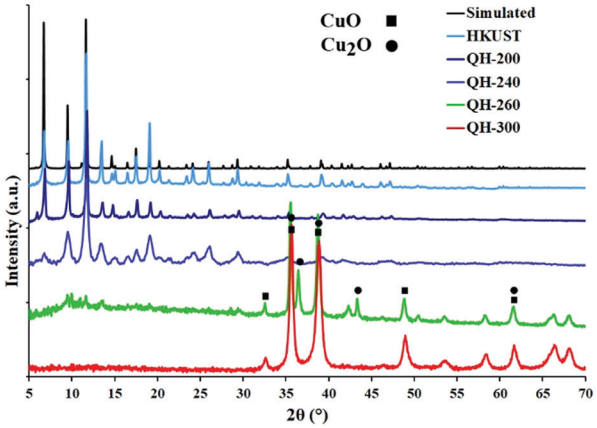

Fig. 2 PXRD patterns of HKUST and QH-*x*.

size, as observed in the transmission electron microscopy images (Fig. 3). The presence of additional meso/macroporosity in QH-240 is also apparent in the images. In this way QH-240 is an interesting intermediate material in which the HKUST-1 structure is partially preserved according to the XRD results, but in which CuO*x* nanoparticles have already started to develop to a large extent. Also, the EPR spectroscopy results (Fig. S5, ESI†) show the presence in QH-240 of about 10% of the Cu^{2+} octahedra present in pristine HKUST-1, meaning that there is a considerable change in the coordination sphere of most of the Cu^{2+} after the thermal deligandation process. This EPR observation is in agreement with the easy H_2O removal in the thermal treatment and also with the partial BTC decarboxylation.

The porosity of the QT-*x* samples was assessed by means of the N_2 sorption isotherm at 77 K. Fig. S6 (ESI†) provides the N_2 adsorption–desorption plots at 77 K. The data show BET specific surface areas of 1182, 913, 160 and 5.6 $m^2\ g^{-1}$ for the type I, (I, IV), IV and V isotherms of HKUST-1, QH-200, QH-240 and QH-260, respectively (Fig. S6 and Table S1, ESI†). In the thermally decomposed samples, the observation of pronounced hysteresis in the adsorption/desorption cycle indicates the generation of cavities. Also, the BJH analysis reveals a significant increase of mesopores in QH-240 after the thermal

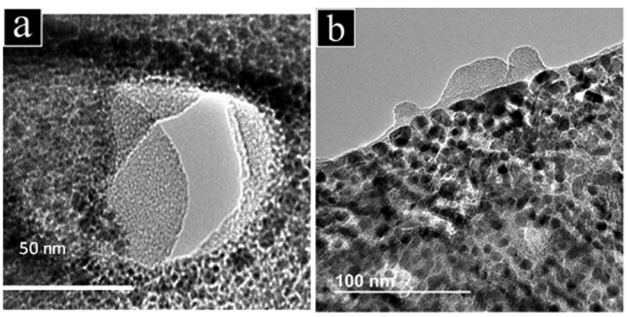

Fig. 3 TEM images of HKUST-1 (a) showing a crystalline particle in the image center surrounded by the resin matrix used to make the tomographic cut and QT-240 (b) in which the formation of CuO_x nanoparticles and the presence of macropores is seen.

Table 1 The TOF values obtained from the hydrolysis of $NaBH_4$ catalyzed by various quasi MOFs determined based on conversions below 30%

Quasi MOF	TOF (mL min^{-1} g^{-1})
No catalyst	1[a]
HKUST	333
QH-200	356
QH-240	6667
QH-260	2300
[b]QH-300	300

Experimental conditions: catalyst mass = 2.5 mg, [$NaBH_4$] = 125 mM and T = 25 °C. [a] (mL min^{-1}). [b] Corresponds to CuO according to the XRD results.

treatment. The presence of micro-/meso-/macropores in QH-240, indicates that partial deligandation defects and vacant sites have been formed in Q-MOF. As a result, the material contains a uniform distribution of coordinatively unsaturated metal centers located in micro- and meso-/macropores that can eventually participate as Lewis acid sites. Macropores can also be observed by TEM.

The hydrolysis of $NaBH_4$ using various QH samples as catalysts was investigated to determine the turnover frequency (TOF) of each sample. The HGRs were performed at 25 °C in water in the absence or presence of the corresponding QH-*x* as the catalyst.

The impact of deligandation temperature over the quasi MOFs, *i.e.* QH-200, QH-240, QH-260 and QH-300 on the HGR for a $NaBH_4$ hydrolysis at 25 °C was evaluated and was compared to the performance of HKUST (Table 1 and Fig. S7, ESI†).

Preliminary controls of the HGR were performed without the catalysts (self-hydrolysis of $NaBH_4$) at 25 °C, and a negligible less than 1 mL min^{-1} H_2 evolution was measured.[25] In contrast, the HGR is accelerated when various QH-*x* samples were used as catalysts. HKUST displays a significantly higher HGR than that for the $NaBH_4$ self-hydrolysis. When thermal treatment was performed on HKUST, the resulting QH-240 and QH-260 samples exhibit an improved catalytic activity with increased TOF values in comparison with the parent HKUST and relevant copper oxide (CuO) at room temperature. The TOF in the presence of the QH-240 and QH-260 catalysts reaches 6667 to 2300 mL min^{-1} g^{-1} at shorter times of 15 and 40 min, respectively, which are respectively almost 20 and 7 times higher than that of HKUST at 25 °C. The QH-240 catalyst shows the highest catalytic HGR efficiency.

The catalytic activity data can be explained based on the BET and TPD results. The TPD results show that the amount and type of acidic sites in QH-240 increased by about 2.2 times compared with the parent HKUST (Fig. S8 and Table S2, ESI†). So, the synergistic effects of the uniform distribution and increased population of active metal catalytic sites across the framework with the concomitant presence of micro-/meso-/macropores (types I and IV and TEM image), together with the limited formation of small Cu_2O/CuO particles are responsible for the excellent catalytic activity. The acid sites as a function of the thermal treatment were measured using NH_3-TPD (see Table S2, ESI†). The results show the increase of medium strength acids sites in QH-240 with respect to the parent HKUST-1.

Investigation of dosage on the catalytic activity indicates a significant effect on TOF value over 2.5 mg of QH-240 catalyst, which reaches a value of 6667 mL min^{-1} g^{-1} (Fig. S9 and Table S3, ESI†). In addition, the logarithmic plot of the H_2 evolution rate *versus* concentration of the QH-240 catalyst exhibits a slope of 1.198, which demonstrates that the $NaBH_4$ hydrolysis by QH-240 is first-order with respect to catalyst concentration (Fig. S10, ESI†).

The influence of the $NaBH_4$ concentration at 25 °C was also investigated (Fig. S11, ESI†) and the results show that the HGR values for 30 min varied remarkably from 250 mL to 495 mL by varying the $NaBH_4$ concentration from 125 mM to 250 mM. All the $NaBH_4$ concentration curves overlap at the beginning, which results in a similar HGR. This phenomenon probably indicates that for the range of concentrations studied, all the catalytic sites are saturated and an additional increase in $NaBH_4$ concentration is not reflected by higher rates. The time–conversion plots show that the catalytic activity of QH-240 is highly stable and efficient, even in a high $NaBH_4$ concentration, and indicates the excellent catalytic performance of QH-240. Also, the slope of the logarithmic plot of HGR *vs.* $NaBH_4$ concentration (0.6) reveals that the catalytic hydrolysis of $NaBH_4$ over QH-240 is essentially first-order with respect to the $NaBH_4$ concentration (Fig. S12, ESI†).

HGR over the QH-240 catalyst was carried out at various temperatures (Fig. S13, ESI†). The activation energy (E_a) was obtained using the Arrhenius equation (eqn (S2)), and gives a value of 58.4 kJ mol^{-1} (Fig. S14, ESI†). This activation barrier is comparable with other related catalysts reported for the HGR using $NaBH_4$ hydrolysis (Table S4, ESI†).[26] In the present case, this low activation energy presumably arises from the synergetic effects of the coordinatively unsaturated copper centers and the coexistence of both meso- and micropores that allow the easy diffusion of water and $NaBH_4$ to the catalytic centers.

The enthalpy and the entropy were estimated to be about 65.21 kJ mol^{-1} and 244.2 (J mol^{-1} K^{-1}), respectively (Fig. S15 and Table S5, ESI†). Also, the activation Gibbs free-energy ($\Delta G\#$) was calculated for temperatures ranging from 298 to 313 K, and provide negative values indicating a spontaneous process. Moreover, the ΔH° of > 0 indicates an endothermic reaction with enhanced disorder ($\Delta S^\circ > 0$).

The catalytic HGR using $NaBH_4$ hydrolysis complies with the model of Langmuir–Hinshelwood (LH)[27] in which the two reagents are adsorbed on the surface of the catalyst. Previous studies demonstrated that, in the generated H_2, one of the hydrogen atoms comes from $NaBH_4$ and another from the O–H bond cleavage of water that is responsible for the rate determining step (RDS), as proven by the isotopic kinetic effect.[28] Hence, the HGR over QH-240 was performed in the $NaBH_4$ + D_2O system (Fig. S16, ESI†). The very high values of the relative k_H to k_D ratio (k_H/k_D = 6.7) firmly support the occurrence of a primary isotopic kinetic effect. The results confirm that the O–H bond of H_2O is cleaved in the RDS using $NaBH_4$ hydrolysis (Fig. S16, ESI†).

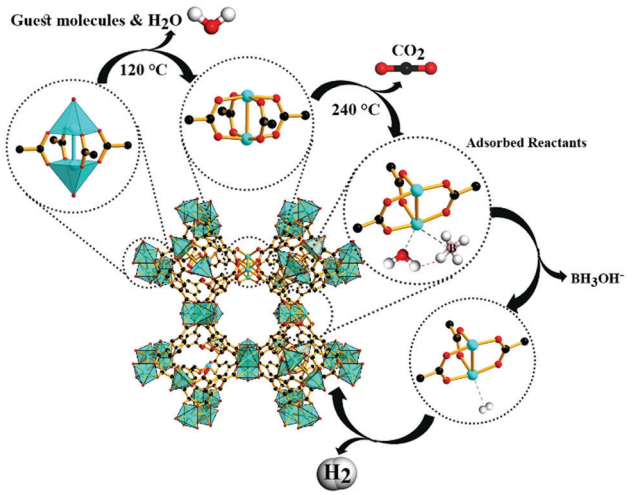

Scheme 1 Mechanistic proposal for HGR over the QH-240 catalyst involving Cu^{2+} and Cu^{+} sites.

As commented on earlier QH-240 exhibits easier mass transfer and a higher density of active Lewis acid sites compared to HKUST-1, and both factors favor BH_4^- and H_2O adsorption on the surface of the catalyst. In addition the Cu^+ sites detected using XPS can also act as active sites. Therefore, in the presence of $Cu^{2+/+}$ sites, coordination of a H_2O molecule and BH_4^- to $Cu^{2+/+}$ will form a copper-dihydride and a BH_3OH^- intermediate. Finally, the product of H_2 is released from the QH-240 surface during the catalytic cycle (Scheme 1).

An excellent catalytic HGR reusability, which nearly maintains the initial activity of the fresh QH-240 catalyst after four reuses, was observed (Fig. S17a, ESI†). The PXRD patterns also confirmed the structural stability of the solid catalyst under the reaction conditions (Fig. S17b, ESI†). Moreover, the ICP analyses exhibited no considerable content of copper in the supernatant, which indicates the high stability of the Q-HKUST MOF.

To put the catalytic activity of QH-240 in a broader context, Table S4 (ESI†) compares the TOF value measured for QH-240 at 25 and 40 °C with that of other Cu and Co benchmark catalysts reported in the literature. As it can be seen, QH-240 exhibits the highest TOF value in the series. Regarding the activation energy that is the other parameter compared, QH-240 has the highest value, although it is comparable to that reported for Co-B@ZIF-8. This comparison clearly shows the potential of the quasi MOF strategy to obtain advanced solid catalysts with improved performance.

In summary, post-synthetic defect engineering of HKUST-1 was performed *via* regulated thermal deligandation to obtain a series of quasi-MOF materials. The Q-HKUST-1 thermolyzed at 240 °C shows high catalytic performance in HGR *via* the hydrolysis of $NaBH_4$. The maximum TOF of 6667 mL min^{-1} g^{-1} was obtained in presence of QH-240 with an activation energy of about 58.4 kJ mol^{-1}. The excellent catalytic behaviour of QH-240 is related to the cooperative effects of the homogeneous and widespread distribution of active copper catalytic sites throughout the lattice and the generation of hierarchical micro- and mesoporous systems. This research would be readily expandable to the preparation of other quasi-MOFs for the H_2 generation process in the industrial field.

This work is based upon research funded by the Iran National Science Foundation (INSF) under project no. 4000089 and Spanish Ministry of Science and Innovation (Severo Ochoa and RTI2018-98237-CO2-1). Also, support for this investigation from Arak University is gratefully acknowledged.

Conflicts of interest

There are no conflicts to declare.

Notes and references

1 B. Zhu, R. Zou and Q. Xu, *Adv. Energy Mater.*, 2018, **8**, 1801193.
2 F. Shi, W. Wu, J. Chen and Q. Xu, *Chem. Commun.*, 2021, **57**, 7011–7014.
3 M. Natali, A. Luisa, E. Iengo and F. Scandola, *Chem. Commun.*, 2014, **50**, 1842–1844.
4 A. C. Yüzer, E. Genc, G. Kurtay, G. Yanalak, E. Aslan, E. Harputlu, K. Ocakoglu, I. Hatay Patir and M. Ince, *Chem. Commun.*, 2021, DOI: 10.1039/D1CC03880J.
5 Y. Fang, S. Wang, G. Lin, X. Wang and F. Huang, *Chem. Commun.*, 2021, **57**, 7946–7949.
6 T. Li, Y. Li, W. Li, S. Jia, X. Chen, X. Zhang and F. Yang, *Chem. Commun.*, 2021, **57**, 7370–7373.
7 N. Sieffert and M. Bühl, *J. Am. Chem. Soc.*, 2010, **132**, 8056–8070.
8 M. Y. Masoomi, A. Morsali, A. Dhakshinamoorthy and H. Garcia, *Angew. Chem., Int. Ed.*, 2019, **58**, 15188–15205.
9 X. Sun, H. Li, Y. Li, F. Xu, J. Xiao, Q. Xia, Y. Li and Z. Li, *Chem. Commun.*, 2015, **51**, 10835–10838.
10 C. Xu, R. Fang, R. Luque, L. Chen and Y. Li, *Coord. Chem. Rev.*, 2019, **388**, 268–292.
11 S. Marx, W. Kleist and A. Baiker, *J. Catal.*, 2011, **281**, 76–87.
12 M.-L. Hu, M. Y. Masoomi and A. Morsali, *Coord. Chem. Rev.*, 2019, **387**, 415–435.
13 A. Bavykina, N. Kolobov, I. S. Khan, J. A. Bau, A. Ramirez and J. Gascon, *Chem. Rev.*, 2020, **120**, 8468–8535.
14 M. Bagheri, M. Y. Masoomi and A. Morsali, *J. Hazard. Mater.*, 2017, **331**, 142–149.
15 D. Ferreira Sanchez, J. Ihli, D. Zhang, T. Rohrbach, P. Zimmermann, J. Lee, C. N. Borca, N. Böhlen, D. Grolimund, J. A. van Bokhoven and M. Ranocchiari, *Angew. Chem., Int. Ed.*, 2021, **60**, 10032–10039.
16 M. Rivera-Torrente, M. Filez, F. Meirer and B. M. Weckhuysen, *Chem. – Eur. J.*, 2020, **26**, 3614–3625.
17 Y. Cheng, X. Xiao, X. Guo, H. Yao and H. Pang, *ACS Sustainable Chem. Eng.*, 2020, **8**, 8675–8680.
18 P. Dong, H. Wang, W. Liu, S. Wang, Y. Wang, J. Zhang, F. Lin, Y. Wang, C. Zhao, X. Duan, S. Wang and H. Sun, *J. Hazard. Mater.*, 2021, **401**, 123423.
19 L. Fan, F. Zhao, Z. Huang, B. Chen, S.-F. Zhou and G. Zhan, *Appl. Catal., A*, 2019, **572**, 34–43.
20 M. Bagheri, M. Y. Masoomi, E. Domínguez and H. García, *ACS Sustainable Chem. Eng.*, 2021, **9**, 10611–10619.
21 Y. Wen, J. Zhang, Q. Xu, X.-T. Wu and Q.-L. Zhu, *Coord. Chem. Rev.*, 2018, **376**, 248–276.
22 J. Chastain and R. C. King Jr., *Handbook of X-ray photoelectron spectroscopy*, PerkinElmer, USA, 1992, vol. 261.
23 Q. Ye, L. Wang and R. T. Yang, *Appl. Catal., A*, 2012, **427–428**, 24–34.
24 F. Severino, J. L. Brito, J. Laine, J. L. G. Fierro and A. L. Agudo, *J. Catal.*, 1998, **177**, 82–95.
25 Y. Kojima, Y. Kawai, H. Nakanishi and S. Matsumoto, *J. Power Sources*, 2004, **135**, 36–41.
26 C. Saka, Ö. Şahin, H. Demir, A. Karabulut and A. Sarikaya, *Energy Sources, Part A*, 2015, **37**, 956–964.
27 S. Wunder, Y. Lu, M. Albrecht and M. Ballauff, *ACS Catal.*, 2011, **1**, 908–916.
28 P. Brack, S. E. Dann and K. G. U. Wijayantha, *Energy Sci. Eng.*, 2015, **3**, 174–188.